Dalton Transactions

Accepted Manuscript

This article can be cited before page numbers have been issued, to do this please use: J. Haeller, E. Mas-Marzá, M. K. Cybulski, R. A. Sanguramath, S. A. Macgregor, M. F. Mahon, C. Raynaud, C. A. Russell and M. K. Whittlesey, *Dalton Trans.*, 2017, DOI: 10.1039/C7DT00117G.

ROYAL SOCIETY OF CHEMISTRY

rsc.li/dalton

View Article Online
DOI: 10.1039/C7DT00117G

Computation Provides Chemical Insight into the Diverse Hydride NMR Chemical Shifts of $[Ru(NHC)_4(L)H]^{0/+}$ Species (NHC = N-heterocyclic carbene; L = vacant, H_2, N_2, CO, MeCN, O_2, P_4, SO_2, H^-, F^- and Cl^-) and their $[Ru(R_2PCH_2CH_2PR_2)_2(L)H]^+$ Congeners

L. Jonas L. Häller,[a] Elena Mas-Marzá,[b] Mateusz K. Cybulski,[b] Rajashekharayya A. Sanguramath,[c] Stuart A. Macgregor,*[a] Mary F. Mahon,[b] Christophe Raynaud,*[d] Christopher A. Russell[c] and Michael K. Whittlesey*[b]

[a]*Institute of Chemical Sciences, Heriot-Watt University, Edinburgh, EH14 4AS, UK*
[b]*Department of Chemistry, University of Bath, Claverton Down, Bath BA2 7AY, UK*
[c]*School of Chemistry, University of Bristol, Cantock's Close, Bristol, BS8 1TS, UK*
[d]*Institut Charles Gerhardt, CNRS 5253, Université de Montpellier, Bâtiment 15, CC 1501, Place Eugène Bataillon, 34 095 Montpellier Cedex 5, France*

View Article Online
DOI: 10.1039/C7DT00117G

Abstract

Relativistic density functional theory calculations, both with and without the effects of spin-orbit coupling, have been employed to model hydride NMR chemical shifts for a series of $[Ru(NHC)_4(L)H]^{0/+}$ species (NHC = N-heterocyclic carbene; L = vacant, H_2, N_2, CO, MeCN, O_2, P_4, SO_2, H^-, F^- and Cl^-), as well as selected phosphine analogues $[Ru(R_2PCH_2CH_2PR_2)(L)H]^+$ (R = ^{i}Pr, Cy; L = vacant, O_2). Inclusion of spin-orbit coupling provides good agreement with the experimental data. For the NHC systems large variations in hydride chemical shift are shown to arise from the paramagnetic term, with high net shielding (L = vacant, Cl^-, F^-) being reinforced by the contribution from spin-orbit coupling. Natural chemical shift analysis highlights the major orbital contributions to the paramagnetic term and rationalizes trends via changes in the energies of the occupied Ru d_π orbitals and the unoccupied $\sigma^*_{Ru\text{-}H}$ orbital. In $[Ru(NHC)_4(\eta^2\text{-}O_2)H]^+$ a δ-interaction with the O_2 ligand results in a low-lying LUMO of d_π character. As a result this orbital can no longer contribute to the paramagnetic shielding, but instead provides additional deshielding via overlap with the remaining (occupied) d_π orbital under the L_z angular momentum operator. These two effects account for the unusual hydride chemical shift of +4.8 ppm observed experimentally for this species. Calculations reproduce hydride chemical shift data observed for $[Ru(^iPr_2PCH_2CH_2P^iPr_2)_2(\eta^2\text{-}O_2)H]^+$ (δ = -6.2 ppm) and $[Ru(R_2PCH_2CH_2PR_2)_2H]^+$ (*ca*. -32 ppm, R = ^{i}Pr, Cy). For the latter, the presence of a weak agostic interaction trans to the hydride ligand is significant, as in its absence (R = Me) calculations predict a chemical shift of -41 ppm, similar to the $[Ru(NHC)_4H]^+$ analogues. Depending on the strength of the agostic interaction a variation of up to 18 ppm in hydride chemical shift is possible and this factor (that is not necessarily readily detected experimentally) can aid in the interpretation of hydride chemical shift data for nominally unsaturated hydride-containing species. The synthesis and crystallographic characterization of the $BAr^F_4^-$ salts of $[Ru(IMe_4)_4(L)H]^+$ (IMe_4 = 1,3,4,5-tetramethylimidazol-2-ylidene; L = P_4, SO_2; Ar^F = 3,5-$(CF_3)_2C_6H_3$) and $[Ru(IMe_4)_4(Cl)H]$ are also reported.

View Article Online
DOI: 10.1039/C7DT00117G

View Article Online
DOI: 10.1039/C7DT00117G

Introduction

Coordinatively unsaturated transition metal hydride complexes, $L_nM–H$, play a central role in many stoichiometric and catalytic transformations[1] and, as a result, their characterization and isolation remains of enduring interest. The often transient nature of such species can make this a challenge and in the absence of definitive crystallographic data much emphasis is placed on the use of spectroscopic techniques to provide structural information. ^{1}H NMR spectroscopy proves a valuable tool in this respect, although the assignment of observed resonances to specific hydride environments is not always straightforward.[2] Thus the direct comparison of pairs of well-defined saturated and unsaturated $L_nM–H$ complexes would be of use in understanding changes that occur upon ligand dissociation and/or coordination.

We have previously reported on the chemistry of the unsaturated square-pyramidal 16e N-heterocyclic carbene (NHC) complexes of the type $[Ru(NHC)_4H]^+$ (NHC = $I^iPr_2Me_2$, IEt_2Me_2, IMe_4),[3] in which the axial hydride ligands display a highly shielded hydride chemical shift at around -41 ppm (Scheme 1).[4] The ability of these $[Ru(NHC)_4H]^+$ fragments to bind small molecules, L, at the vacant coordination site trans to H varies considerably according to the NHC substituents.[5] Thus only $[Ru(I^iPr_2Me_2)_4H]^+$ forms a stable adduct with O_2, $[Ru(IMe_4)_4H]^+$ and $[Ru(IEt_2Me_2)_4H]^+$ both reversibly bind N_2 and H_2, and all three complexes irreversibly bind CO. For the saturated 18e $[Ru(NHC)_4(L)H]^+$ species with L = H_2, N_2 and CO the hydride signals appear in the range δ = -4 ppm to δ = -10 ppm. However, the hydride in $[Ru(I^iPr_2Me_2)_4(\eta^2\text{-}O_2)H]^+$ resonates at δ = + 4.8 ppm. Such highly deshielded hydride chemical shifts have been reported and rationalized for d^{10} and d^0 systems[6] but are unusual for intermediate electron counts.

View Article Online
DOI: 10.1039/C7DT00117G

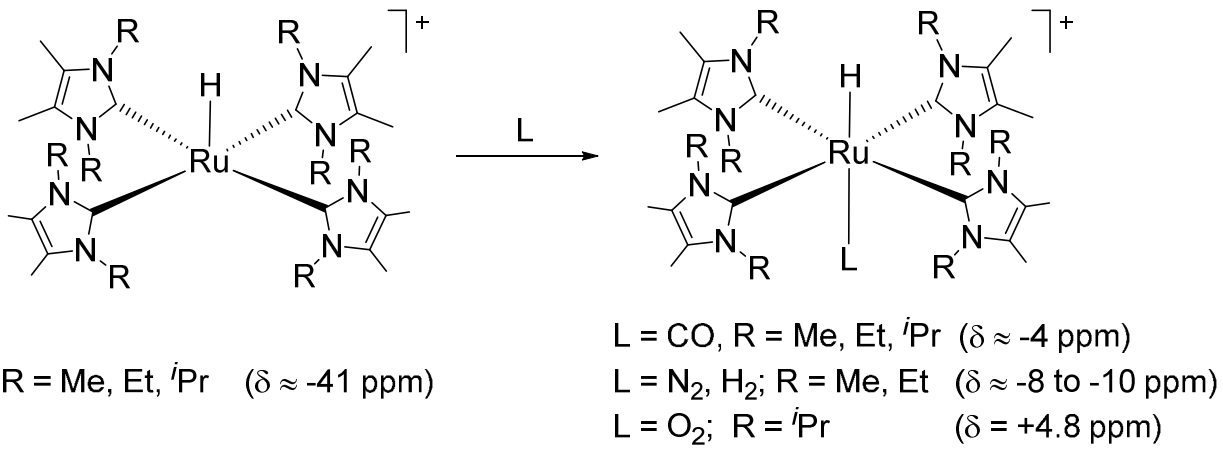

Scheme 1

Related to these $[Ru(NHC)_4H]^+$ systems are the 16e square-pyramidal complexes of the form $[Ru(R_2PCH_2CH_2PR_2)_2H]^+$ (R = Cy, ^{i}Pr) for which the hydride chemical shifts appear around δ = -32 ppm.[7] These species can also bind a range of ligands including O_2, and for the $[Ru(R_2PCH_2CH_2PR_2)_2(\eta^2\text{-}O_2)H]^+$ adducts the hydride chemical shift is observed at δ = -5 ppm. Thus for the NHC systems, the hydride chemical shift changes by over 45 ppm upon O_2 binding, whereas for the apparently closely related phosphine systems this span is reduced to only 27 ppm.

The last two decades have seen significant progress in the use of theoretical methods to model the hydride chemical shifts of L_nM–H species.[8] In 1996 Ziegler and co-workers applied density functional theory (DFT) calculations to model the hydride chemical shifts of 18e transition metal carbonyl hydrides.[9] Building on early work by Buckingham and Stephens,[10] this paper outlined the mechanism by which the paramagnetic term contributes to the negative chemical shifts typical of most L_nM-H species. Subsequent studies have appeared on a range of L_nM–H complexes[11] and clusters[12] and have in general provided good qualitative agreement between experimental and computed hydride chemical shifts.

View Article Online
DOI: 10.1039/C7DT00117G

Relativistic effects also play an important role in determining hydride chemical shifts.[13] Ziegler and co-workers included scalar relativistic corrections in their study of $[Re(CO)_5H]$,[9] while more recently the inclusion of spin-orbit coupling effects has been shown to improve the agreement of computed and experimental hydride chemical shifts.[6a, 14] Using relativistic 4-component DFT calculations, Hrobárik, Kaupp and co-workers[6a] showed that spin-orbit coupling can be particularly important for unsaturated 16e species, and that this effect could be significant not only for complexes of the 3rd row transition metals but also for their 1st and 2nd row congeners. Thus for the series of Group 9 $[M(PMe_3)_2Cl_2H]$ complexes calculated hydride chemical shifts were -35.3(-17.2) ppm, -25.6(-13.0) ppm and -43.2(-28.7) ppm for M = Co, Rh and Ir respectively, where the contributions from spin-orbit coupling are given in parenthesis.

In the following DFT calculations are used to model the observed hydride chemical shift data of 16e $[Ru(IMe_4)_4H]^+$ and $[Ru(dippe)_2H]^+$ species (dippe = $^iPr_2PCH_2CH_2P^iPr_2$) and the η^2-O_2 adducts $[Ru(I^iPr_2Me_2)_4(\eta^2\text{-}O_2)H]^+$ and $[Ru(dippe)_2(\eta^2\text{-}O_2)H]^+$. The modelling study is extended to include a range of 18e neutral and cationic $[Ru(IMe_4)_4(L)H]^{0/+}$ species and as part of this we report the synthesis and full characterization of $[Ru(IMe_4)_4(P_4)H]BAr^F{}_4$, **1**, $[Ru(IMe_4)_4(SO_2)H]BAr^F{}_4$, **2**, and $[Ru(IMe_4)_4(Cl)H]$, **3**, for the first time. The calculations provide good agreement with the experimental data and again highlight the importance of the paramagnetic and spin-orbit coupling contributions in determining the hydride chemical shifts. A Natural Chemical Shift (NCS) analysis then provides chemical insight into how the paramagnetic and spin-orbit terms vary with the occupation of the site trans to hydride and how this can be understood with reference to the underlying electronic structure. The NCS approach has recently proved useful in understanding the ^{13}C NMR chemical shift associated with alkylidene ligands in a range of d^0 olefin metathesis catalysts.[15]

View Article Online
DOI: 10.1039/C7DT00117G

Results and Discussion.

Synthesis and Characterization of $[Ru(IMe_4)_4(L)H][BAr^F_4]$ (L = P_4, 1, SO_2, 2) and $[Ru(IMe_4)_4(Cl)H]$, 3.

Treatment of THF solutions of the BAr^F_4 salt of $[Ru(IMe_4)H]^+$ with an equivalent of white phosphorus led to a rapid colour change from purple to orange resulting from the formation of $[Ru(IMe_4)_4(P_4)H]BAr^F_4$ (**1**). An X-ray crystal structure (Figure 1a) showed η^1-coordination of the P_4 cage trans to the hydride ligand. The Ru-P distance (2.3029(8) Å) is slightly shorter than in either of the chelating phosphine analogues, $[Ru(Me_2PCH_2CH_2PMe_2)_2(P_4)H]BF_4$ (2.3215(17)/2.3270(16) Å) and $[Ru(Ph_2PCH_2CH_2PPh_2)_2(P_4)H]BF_4$ (2.3449(12) Å), which also feature a trans H-Ru-P geometry.[16] The P_4 ligand in **1** exhibited fluxionality: at room temperature, the Ru-H resonance (δ -5.13) appeared as a doublet ($^1J_{H\text{-}P}$ = 264.5 Hz), although upon cooling to 278 K, this resolved into the anticipated doublet of quartets, with $^2J_{H\text{-}P}$ and $^3J_{H\text{-}P}$ splittings of 266.1 and 11.0 Hz respectively. The 278 K $^{31}P\{^1H\}$ NMR spectrum showed low frequency quartet (δ -394.6) and doublet (δ -468.6) signals, characteristic for bound and unbound phosphorus atoms in metal-P_4 complexes.[17, 18]

Exposure of $[Ru(IMe_4)H]BAr^F_4$ to SO_2 gave $[Ru(IMe_4)_4(SO_2)H]BAr^F_4$ (**2**) in time of mixing. A combination of X-ray crystallography (Figure 1b) and IR spectroscopy confirmed that the SO_2 ligand was bound in a coplanar mode[19] with the long Ru-S distance of 2.1753(16) Å presumably a result of being trans to the hydride ligand.[20] The Ru-H chemical shift of **2** was observed at δ -4.51.

View Article Online
DOI: 10.1039/C7DT00117G

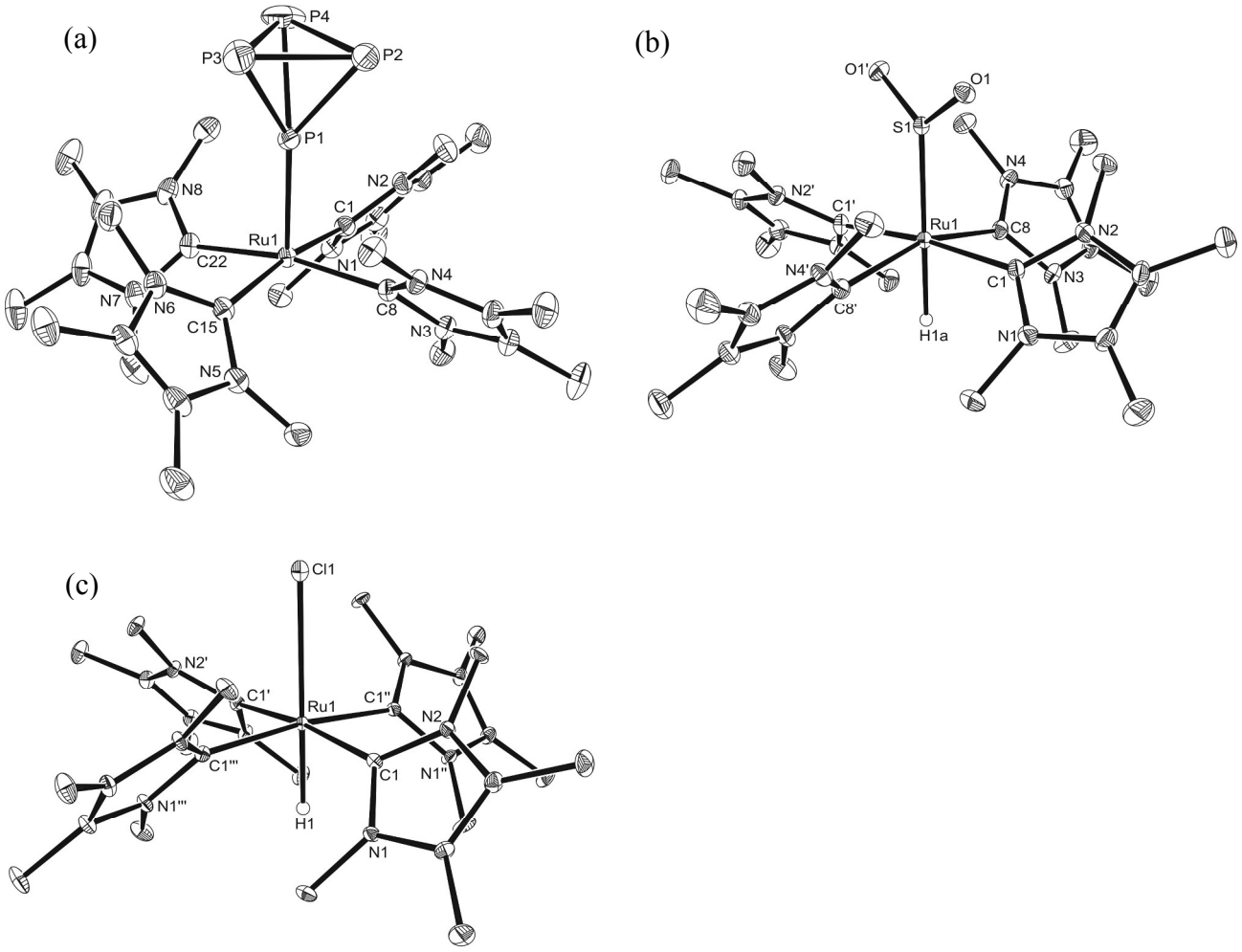

Figure 1. Molecular structures of (a) **1**, (b) **2** and (c) **3**. Minor disordered component and hydrogen atoms, with the exception of the hydride ligand, are omitted for clarity in **2** and atoms with primed labels are related to those in the asymmetric unit by the $1 - x, y, 2 - z$ symmetry operation. Atoms with primed, double-primed and triple-primed labels in **3** are related to those in the asymmetric unit by the $1 - x, 1 - y, z$, $1 - y, x, z$ and $y, 1 - x, z$ symmetry operations, respectively, and hydrogen atoms, with the exception of the hydride ligand, are omitted for clarity. Selected bond lengths (Å) and angles (°). **1**: Ru(1)-C(1) 2.113(3), Ru(1)-C(8) 2.095(3), Ru(1)-C(15) 2.097(3), Ru(1)-C(22) 2.110(3), Ru(1)-P(1) 2.3029(8), C(1)-Ru(1)-C(15) 170.07(11). **2**: Ru(1)-C(1) 2.116(4), Ru(1)-C(8) 2.128(4), Ru(1)-S(1) 2.1753(16), C(1)-Ru(1)-C(1′) 173.2(2). **3**: Ru(1)-C(1) 2.089(3), Ru(1)-Cl(1) 2.751(3), C(1)-Ru(1)-C(1′) 172.5(2). Thermal ellipsoids are represented at 30% probability.

View Article Online
DOI: 10.1039/C7DT00117G

Formation of the neutral hydride chloride complex $[Ru(IMe_4)_4(Cl)H]$ (**3**) was accomplished either by reaction of $[Ru(IMe_4)_4H_2]$ with an equimolar quantity of benzyl chloride in THF at room temperature or, on a more synthetically viable scale, by heating $[Ru(PPh_3)_3(Cl)H]$ in THF for 1 h at 343 K with 4.5 equivalents of free IMe_4. The choice of solvent in these reactions was critical, as the complex was only sparingly soluble in THF, but completely insoluble in solvents such as benzene or toluene.[21] The ^1H NMR spectrum of **3** showed a highly shielded Ru-H hydride resonance at δ -22.56. In addition, an unusually long Ru-Cl bond length was determined in the X-ray crystal structure (Figure 1c): at 2.751(3) Å this is ca. 0.15 Å longer than the longest distance reported for structurally characterized $[Ru(P\text{-}P)_2(Cl)H]$ complexes in the literature,[22] and is consistent with a loosely bound chloride ligand.

Computational Studies

DFT calculations were performed to model and rationalize the observed hydride chemical shifts in a series of $[Ru(IMe_4)_4(L)H]^+$ cations (L = vacant, H_2, N_2, CO, MeCN,[5] O_2,[4] P_4 and SO_2) and the related neutral $[Ru(IMe_4)_4(L)H]$ species (L = H^-,[23] F^- and Cl^-). These provide a series of complexes in which the trans ligand L exhibits a range of donor and acceptor properties and so provides the opportunity to rationalize trends in hydride chemical shifts. The related phosphine cations $[Ru(dippe)_2H]^+$ and $[Ru(dippe)_2(\eta^2\text{-}O_2)H]^+$ will also be considered.

$[Ru(IMe_4)_4(L)H]^+$: Computed Structures. Previously BP86 calculations on $[Ru(IMe_4)_4(L)H]^+$ species (L = vacant, H_2, N_2, CO[5] and O_2[4]) provided good agreement with experimental metrics and the same approach was used here to compute structures for the remaining $[Ru(IMe_4)_4(L)H]^{0/+}$ species. Selected computed data are presented in Table 1 and compared with the available structural data and their experimentally determined hydride chemical shifts. The Ru-P distance computed in **1** and the Ru-

View Article Online
DOI: 10.1039/C7DT00117G

S distance in **2** are both slightly overestimated by *ca*. 0.08 Å although the very long Ru-Cl distance observed experimentally is **3** well reproduced. The high trans influence hydride ligand will certainly play a role in labilizing the Cl^- ligand in **3** and this may be further facilitated by close Cl···H-C contacts to four H atoms on the IMe_4 *N*-Me substituents. Indeed computed NBO charges (q_{Cl} = -0.66; q_H = +0.29) do suggest a degree of $Cl^{\delta-}\cdots H^{\delta+}$ electrostatic stabilization and this was supported by a non-covalent interaction (NCI) analysis[24] that highlights areas of non-covalent stabilization between the chloride and each of these hydrogens (see Figure S9, ESI). The computed structure of $[Ru(IMe_4)_4(F)H]$ similarly captures the long Ru-F distance and again highlights four short F···H-C contacts of 1.87 Å.[25]

L	Ru-H_{calc}	Ru-L_{calc}	Ru-L_{exp}	δ^{exp}
Vacant	1.55	-	-	-40.7[a]
F^-	1.62	2.28	2.3070(18)	-23.2[b]
Cl^-	1.61	2.72	2.751(3)	-22.6
MeCN	1.63	2.06		-14.5[a]
N_2	1.64	1.97		-10.2[a]
H_2	1.62	1.70[c]		-9.3[a]
H^-	1.71	1.71	1.69(3)[d]	-7.5[d]
P_4	1.61	2.38	2.3031(8)	-5.1
SO_2	1.62	2.25	2.1804(15)[e]	-4.5
CO	1.69	1.89	1.983(6)[a, f]	-4.0[a]
O_2	1.61	1.98[c]	1.985(3)[g]	+4.8[g]

Table 1. Selected calculated and experimental data for neutral and cationic $[Ru(IMe_4)_4(L)H]^{0/+}$ species with bond distances in Å and hydride chemical shifts in ppm. [a]Ref 5; [b]Ref 25; [c]distance to the

View Article Online
DOI: 10.1039/C7DT00117G

midpoint of the H_2/O_2 ligand; [d]Ref 23; [e]average of two molecules in the unit cell; [f]data are for $[Ru(I^iPr_2Me_2)_4(CO)H]^+$; [g]Ref 4; data are for $[Ru(I^iPr_2Me_2)_4(\eta^2\text{-}O_2)H]^+$.

Over the series of neutral and cationic $[Ru(IMe_4)_4(L)H]^{0/+}$ complexes computed Ru-H distances range from 1.55 Å in 5-coordinate $[Ru(IMe_4)_4H]^+$ to 1.71 Å in $[Ru(IMe_4)_4H_2]$[26] and there appears to be little relationship between the computed Ru-H distances and the observed hydride chemical shifts. For example, both $[Ru(IMe_4)_4(\eta^2\text{-}O_2)H]^+$ and $[Ru(IMe_4)_4(Cl)H]$ have computed Ru-H distances of 1.61 Å, but the hydride chemical shift for the O_2 adduct is shifted by 28 ppm relative to that of **3**.

$[Ru(IMe_4)_4(L)H]^{0/+}$: **Computed hydride chemical shifts.** Hydride chemical shifts for the $[Ru(IMe_4)_4(L)H]^{0/+}$ species using the BP86-optimized geometries were calculated using three different relativistic Hamiltonians: (i) through the ZORA approximation using the ADF program with the B1PW91 hybrid density functional (δ_{iso}^{ZORA}); (ii) with ADF but *without* a correction for spin-orbit coupling effects (δ_{iso}^{1C}) and; (iii) with a X2C Hamiltonian using the Dirac program with the B3PW91 hybrid density functional (δ_{iso}^{X2C}). The results are plotted in Figure 2 and show all three approaches provide an excellent correlation with experiment (R^2 values > 0.98). However, significantly improved absolute agreement is found upon including spin-orbit coupling, these plots having gradients of 0.94 (δ_{iso}^{ZORA} and δ_{iso}^{X2C}) compared to 0.65 in the absence of this factor (δ_{iso}^{1C}). The contribution from spin-orbit coupling therefore becomes more significant as the chemical shift becomes more negative, with particularly large contributions for L = Cl^- and F^- (> 5 ppm) and for 5-coordinate $[Ru(IMe_4)_4H]^+$ (> 11 ppm). Full listings of computed hydride chemical shift data are provided in the Supporting Information (Table S2).

View Article Online
DOI: 10.1039/C7DT00117G

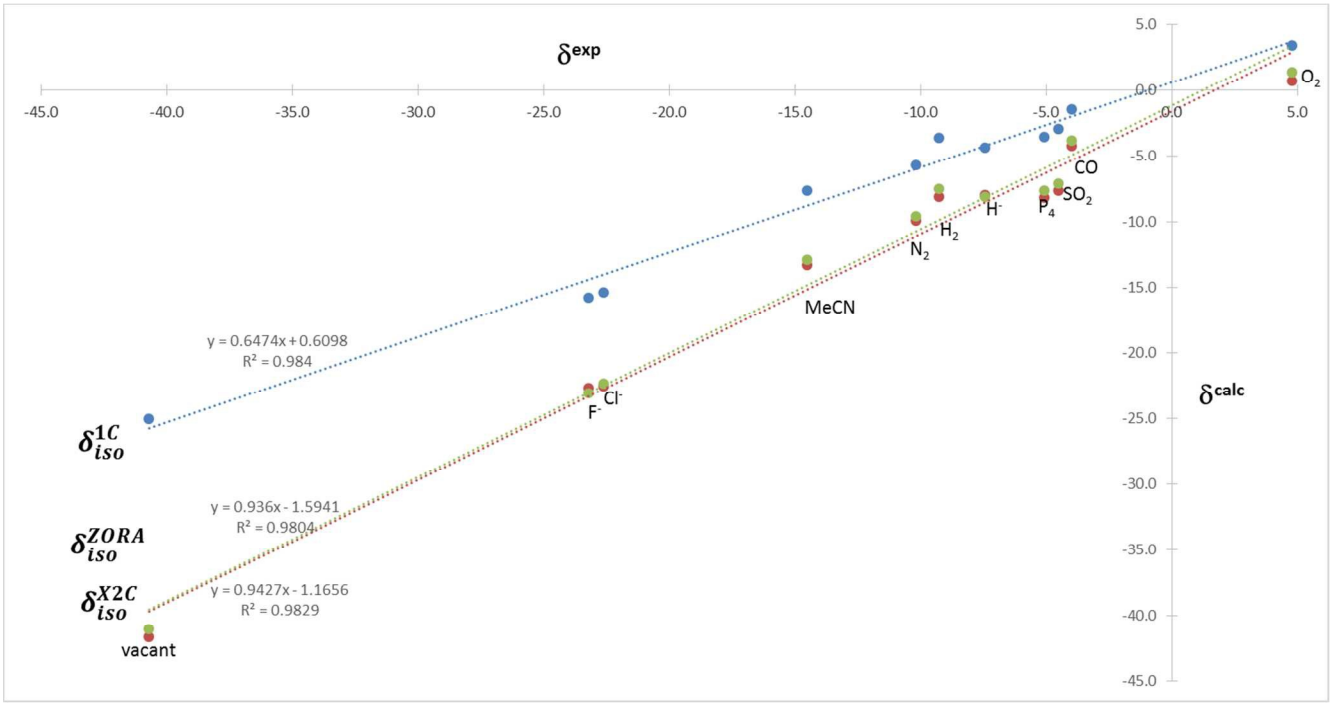

Figure 2. Plots of experimental (δ^{exp}) vs. computed chemical shifts (δ^{calc}) for $[Ru(IMe_4)_4(L)H]^{0/+}$ species, at the δ_{iso}^{1C}, δ_{iso}^{ZORA} and δ_{iso}^{X2C} levels of approximation.

In order to analyze the trends in the computed chemical shifts, a subset of the $[Ru(IMe_4)_4(L)H]^{0/+}$ species was selected to cover the full range of hydride chemical shifts (i.e. from L = vacant to L = O_2) and to monitor the effects of introducing a simple σ-donor (L = H^-), a π-donor (L = Cl^-) and a π-acceptor ligand (L = CO). The isotropic chemical shift for a given system, δ_{iso}, is related to the isotropic shielding of the hydrogen nucleus relative to that of a hydrogen in $SiMe_4$ (TMS):

$$\delta_{iso} = \sigma_{iso}^{TMS} - \sigma_{iso}$$

where σ_{iso} is itself an average of the three principal components of the rank-2 shielding tensor. For these $[Ru(IMe_4)_4(L)H]^{0/+}$ systems the three components are either parallel ($\sigma_{||}$) or perpendicular ($\sigma_{\perp}$) to the Ru-H bond and for L = vacant, H^-, Cl^- and CO the C_4 symmetry means these two $\sigma_{\perp}$ terms are equivalent, i.e.:

View Article Online
DOI: 10.1039/C7DT00117G

$$\sigma_{iso} = \frac{1}{3}(\sigma_{11} + \sigma_{22} + \sigma_{33}) \quad = \quad \frac{1}{3}\sigma_{||} + \frac{2}{3}\sigma_{\perp}$$

Within the GIAO scheme, σ_{iso} can also be expressed as:

$$\sigma_{iso} = \sigma_{iso}^{d} + \sigma_{iso}^{p} + \sigma_{iso}^{so}$$

where σ_{iso}^{d} is the diamagnetic contribution, σ_{iso}^{p} the paramagnetic contribution and σ_{iso}^{so} the contribution from spin-orbit coupling. Each of these terms will also have parallel and perpendicular components.

Computed values for σ_{iso}, σ_{iso}^{d}, σ_{iso}^{p} and σ_{iso}^{so} for the selected $[Ru(IMe_4)_4(L)H]^{0/+}$ species are provided in Table 2, along with the $\sigma_{||}$ and $\sigma_{\perp}$ contributions for the latter three terms. As noted by others,[9] σ_{iso}^{d} (and its components) show little variation and the trend in σ_{iso} is dominated by changes in σ_{iso}^{p} which are then augmented by σ_{iso}^{so}.

L	σ_{iso}	σ_{iso}^{d}	$\sigma_{||}^{d}$	$\sigma_{\perp}^{d}$	σ_{iso}^{p}	$\sigma_{||}^{p}$	$\sigma_{\perp}^{p}$	σ_{iso}^{so}	$\sigma_{||}^{SO}$	$\sigma_{\perp}^{so}$
Vacant	**73.3**	**27.8**	39.9	21.8	**28.5**	-12.8	49.2	**16.9**	-1.5	26.1
Cl^-	**54.1**	**27.8**	38.9	22.3	**20.0**	-10.4	35.2	**6.3**	-0.5	9.7
H^-	**39.6**	**26.1**	35.9	21.2	**10.5**	-7.8	19.7	**3.0**	-0.2	4.7
CO	**35.8**	**25.4**	34.5	20.8	**8.4**	-7.4	16.3	**2.1**	-0.2	3.3
O_2	**30.9**	**25.2**	35.4	17.0/23.2	**3.8**	-34.6	15.7/30.3	**2.0**	-0.7	-3.7/10.5

Table 2. Calculated values (ZORA, B1PW91) for σ_{iso}, σ_{iso}^{d}, σ_{iso}^{p} and σ_{iso}^{so} for selected $[Ru(IMe_4)_4(L)H]^{0/+}$ species, along with $\sigma_{||}$ and $\sigma_{\perp}$ contributions for σ_{iso}^{d}, σ_{iso}^{p} and σ_{iso}^{so}. For L = O_2 two components are provided for the perpendicular terms due to the lower symmetry of the system.

σ_{iso}^{p} is related to the expression:

View Article Online
DOI: 10.1039/C7DT00117G

$$\frac{\langle\varphi_{vac}|\hat{L}_i|\varphi_{occ}\rangle\langle\varphi_v|\hat{L}_i/r^3|\varphi_{occ}\rangle}{\Delta E_{vac-occ}}$$

and the key implications of this are outlined below, following Ziegler and co-workers:[9]

(i) σ^p_{iso} arises from the ability of the applied magnetic field to induce a circulation of charge initially residing in the occupied orbitals, φ_{occ}, by making use of the vacant orbitals, φ_{vac}.

(ii) This process is governed by the angular momentum operator, $\hat{L}_i$, where $i = x$, y and z: these correspond to the axes of the principal components of the shielding tensor and are therefore either perpendicular (x, y) or parallel (z) to the Ru-H bond.

(iii) σ^p_{iso} is inversely proportional to the difference in energy between φ_{occ} and φ_{vac} and so is dominated by molecular orbitals around the HOMO-LUMO gap.

(iv) For transition metal hydrides the proximity of the hydride to the metal centre means that its shielding tensor is strongly influenced by ring currents induced within the set of metal-based orbitals. A ring current at the metal which is perpendicular to the Ru-H direction induces a magnetic field that reinforces the external field and so deshields the hydrogen nucleus (σ_{iso} is negative and $\Delta\sigma$ is positive). In contrast, a metal ring current in a plane containing the M-H bond induces a magnetic field that opposes the external field and so increases the shielding of the hydrogen nucleus (σ_{iso} is positive and $\Delta\sigma$ is negative).

Figure 3 provides a qualitative picture of the relevant metal-based orbitals of square-pyramidal $[Ru(IMe_4)_4H]^+$. This features three low-lying occupied d-orbitals, d_{xz} and d_{yz} (d_π with respect to the Ru-H axis) and the d_{xy} orbital. To higher energy lie $\sigma^*_{Ru\text{-}H}$, an unoccupied antibonding Ru-H orbital featuring a mixture of d_{z^2}, p_z and s Ru character and, above this, the $d_{x^2\text{-}y^2}$ orbital which is antibonding

View Article Online
DOI: 10.1039/C7DT00117G

with respect to the four IMe_4 ligands. Coupling between the occupied and vacant orbitals under $\hat{L}_i$ is governed by Cornwall's model of orbital rotations:[27] the rotated orbital $\hat{L}_z|d_{xy}>$ has significant overlap with the $d_{x^2-y^2}$ orbital, while $\hat{L}_y|d_{xz}>$ and $\hat{L}_x|d_{yz}>$ both overlap with σ^*_{Ru-H}. These couplings will be labelled $\{d_{xy}|d_{x^2-y^2}\}$ and $\{d_\pi|\sigma^*_{Ru-H}\}$ respectively in the following.

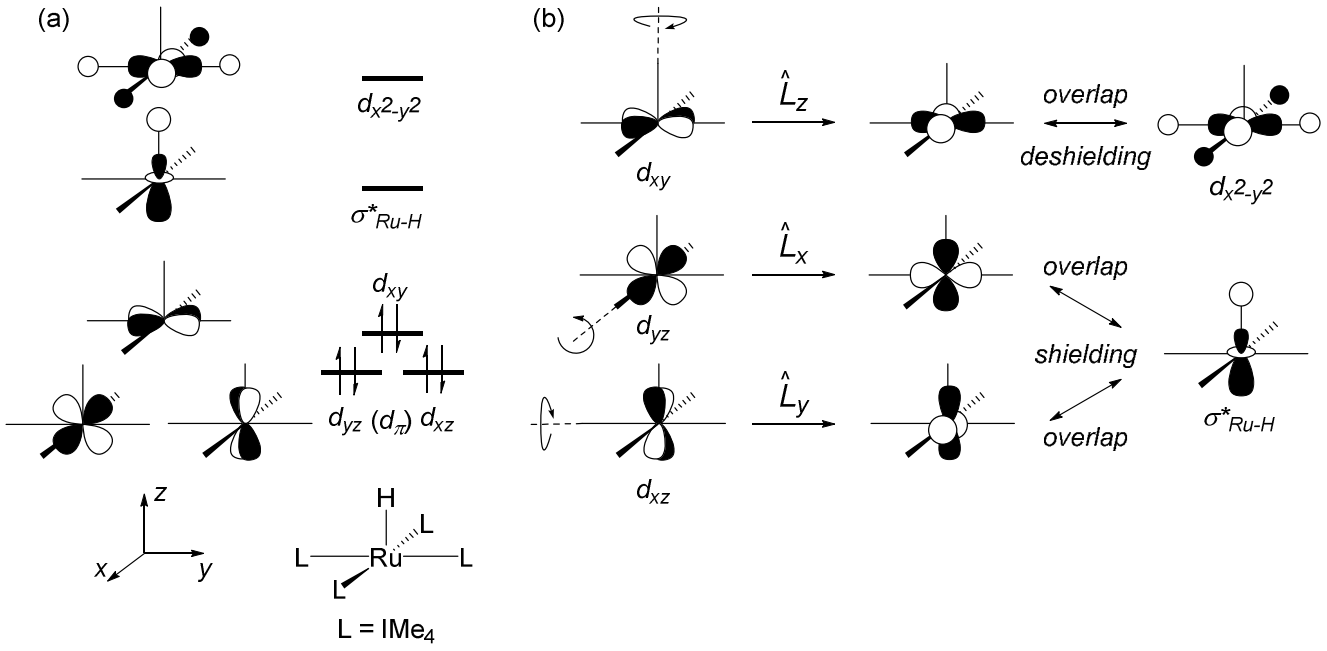

Figure 3. (a) Relevant metal-based molecular orbitals of $[Ru(IMe_4)_4H]^+$; (b) coupling of metal-based orbitals via the angular momentum operator and their contribution to the paramagnetic term.

The relationship between the electronic structure and the calculated shielding tensors was probed using the Natural Chemical Shift (NCS) analysis based on the scalar relativistic natural localized molecular orbitals.[27a, 28] The NCS analysis, which is implemented in the ADF program and is hence applied to the δ_{iso}^{ZORA} data, allows contributions from localized occupied orbitals to be identified and the most important of these are detailed in Table 3 for σ_{iso}^{p} and σ_{iso}^{so}.

View Article Online
DOI: 10.1039/C7DT00117G

L	$\sigma_{\parallel}^{p}$		$\sigma_{\perp}^{p}$		$\sigma_{\parallel}^{so}$	$\sigma_{\perp}^{so}$
	d_{π}	d_{xy}	d_{π}	d_{xy}	σ^{*}_{Ru-H}	σ^{*}_{Ru-H}
Vacant	-1.7	-15.5	49.5	0.9	-1.0	9.6
Cl^-	-2.2	-13.7	33.0	1.0	-0.3	4.3
H^-	-2.0	-10.4	16.1	1.0	-0.1	2.0
CO	-0.5	-13.6	10.9	0.7	0.0	0.1
O_2	-25.3[a]	-17.1	26.5[a, b]	2.3[c]	-0.2	2.5[c]

Table 3. NCS analysis of the contributions (ppm) to σ_{iso}^{p} and σ_{iso}^{so} for selected $[Ru(IMe_4)_4(L)H]^{0+}$ species. [a]only d_{xz} contributes, see text; [b]d_{xz} contributes 0.8 ppm to shielding via rotation about the *x*-axis; [c] the average of two contributions due to rotation about the *x*- and *y*-axes is given; see Figure 4 for orientation.

For $[Ru(IMe_4)_4H]^+$ the major contributions are a deshielding from $\{d_{xy}|d_{x^2-y^2}\}$ ($\sigma_{||}^{p}$, -15.5 ppm) and a shielding from $\{d_{\pi}|\sigma^{*}_{Ru-H}\}$ ($\sigma_{\perp}^{p}$, 49.5 ppm). The small energy gap between the d_{π} and σ^{*}_{Ru-H} orbitals means that the latter shielding is the more significant term. The resultant net shielding arising from σ_{iso}^{p} is then reinforced by σ_{iso}^{so}, contributing to the $\sigma_{\perp}$ term ($\sigma_{\perp}^{so}$, 9.6 ppm). As with the paramagnetic term, the spin-orbit contribution also appears in the sum-over-unoccupied orbitals part of the Ramsey-type equations and the mechanism by which the spin-orbit term operates has been discussed by Kaupp and co-workers.[29] In the presence of an external magnetic field, spin-orbit coupling induces a degree of spin polarization via mixing of some triplet character into the singlet ground state. σ-π mixing between the Ru d_{π} and the Ru-H σ* orbitals allows this spin polarization to be transferred to the hydrogen where it is transmitted by the relativistic analogue of the Fermi-contact and spin-dipole mechanisms on the hydrogen centre. This coupling mechanism necessarily involves s-orbital character at hydrogen and this explains the dominance of the antibonding σ^{*}_{Ru-H} in the spin-orbit contribution to the hydride shielding for the $\sigma_{\perp}$ term.

View Article Online
DOI: 10.1039/C7DT00117G

The computed changes in $\sigma_{\perp}^{p}$ and $\sigma_{||}^{p}$ upon introducing a sixth ligand can be qualitatively rationalized by considering the effects on the orbitals in Figure 3. For L = H^-, Cl^- and CO σ-donation occurs into $\sigma^*_{Ru\text{-}H}$, destabilizing that orbital and hence reducing the shielding contribution of the $\{d_{\pi}|\sigma^*_{Ru\text{-}H}\}$ term to $\sigma_{\perp}^{p}$. For L = H^- this is the major effect and, reinforced by the high trans influence of hydride, results in a significant decrease in $\sigma_{\perp}^{p}$ from 49.5 ppm to 16.1 ppm. The d_{xy} and $d_{x^2\text{-}y^2}$ orbitals are both orthogonal to the H^- 1s orbital and so to a first approximation are unaffected: accordingly the $\{d_{xy}|d_{x^2\text{-}y^2}\}$ deshielding contribution changes by only 5 ppm, presumably reflecting changes in orbital overlap.

Cl^- has a much lower trans influence than H^-, in particular at the long Ru-Cl distance of 2.72 Å calculated for $[Ru(IMe)_4(Cl)H]$. The destabilization of $\sigma^*_{Ru\text{-}H}$ will therefore be reduced; moreover any π-donation from Cl^- will also destabilize the d_{π} orbitals. These factors suggest a relatively small d_{π} to $\sigma^*_{Ru\text{-}H}$ energy gap is retained and so explain the significant $\{d_{\pi}|\sigma^*_{Ru\text{-}H}\}$ shielding contribution of 33.0 ppm to $\sigma_{\perp}^{p}$. In contrast, the high trans influence CO ligand will both destabilize $\sigma^*_{Ru\text{-}H}$ and stabilize the d_{π} orbitals through π-back donation. The d_{π}-$\sigma^*_{Ru\text{-}H}$ energy gap is therefore large and as a result the $\{d_{\pi}|\sigma^*_{Ru\text{-}H}\}$ shielding contribution of 10.9 ppm to $\sigma_{\perp}^{p}$ is even smaller than for H^-.

For $[Ru(IMe)_4(\eta^2\text{-}O_2)H]^+$ the availability of two sets of π-MOs on the O_2 ligand (π_1/π^*_1 and π_2/π^*_2) causes significant changes in electronic structure (see Figures 4(a) and (b)). The π-bonding orbitals of O_2 provide both a σ-donor (π_1: destabilization of $\sigma^*_{Ru\text{-}H}$) and a π-donor orbital (π_2: destabilization of d_{xz}). Of the antibonding orbitals, π^*_1 overlaps with d_{yz} and the resultant antibonding combination, d_{yz} - π^*_1, forms the LUMO of the system. π^*_2 forms δ-type orbitals, $d_{xy} \pm \pi^*_2$, and the relatively weak δ-overlap means that these orbitals remain close in energy and that the bonding and antibonding

View Article Online
DOI: 10.1039/C7DT00117G

combinations are heavily located on the metal and the O_2 ligand respectively. The d_{xy} - π^*_2 combination becomes the HOMO of the system and implies a degree of electron transfer from Ru to O_2.

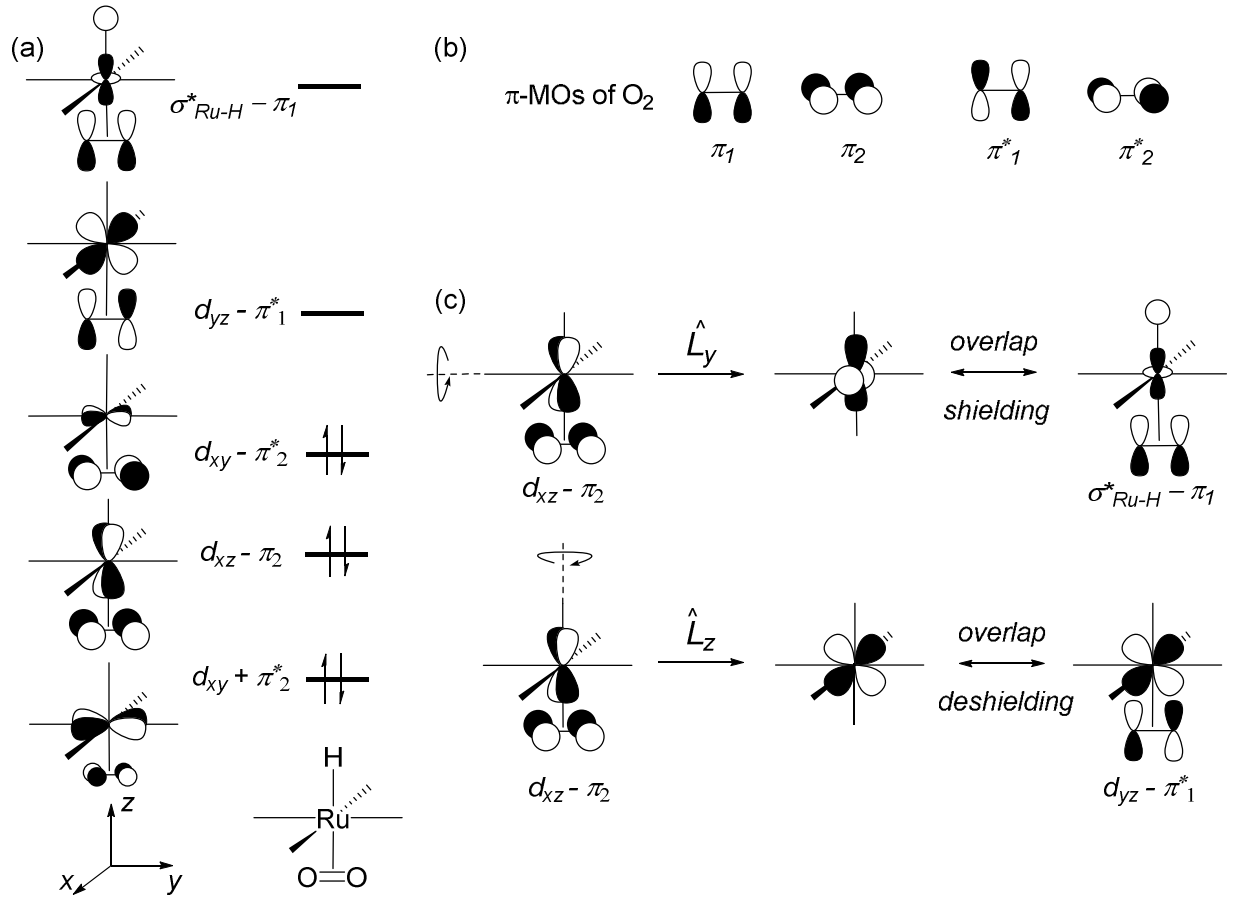

Figure 4. (a) Selected metal-based orbitals for $[Ru(IMe_4)_4(\eta^2\text{-}O_2)H]^+$; (b) π-MOs of O_2; (c) coupling of metal-based orbitals via the angular momentum operator and their contribution to the paramagnetic term; for the rotated orbitals only the metal-based component is indicated for clarity.

The destabilization of the d_{yz} orbital to form the LUMO has two consequences for σ^p_{iso} (Figure 4(c)). Firstly, the equivalent orbital was occupied in the other $[Ru(IMe)_4(L)H]^{0/+}$ species and so contributed to $\sigma^p_\perp$ through coupling with $\sigma^*_{Ru\text{-}H}$. This is therefore lost in $[Ru(IMe)_4(\eta^2\text{-}O_2)H]^+$ in which only the d_{xz} – π_2 contributes to shielding (26.5 ppm, Table 3). Secondly, d_{xz} – π_2 can also couple though L_z with d_{yz} – π^*_1 and the small energy gap means this contributes a significant deshielding to $\sigma^p_{||}$ (-25.3 ppm). The

View Article Online
DOI: 10.1039/C7DT00117G

cumulative effect of these two factors (reduced shielding and increased deshielding) accounts for the unusually low-field chemical shift observed experimentally for $[Ru(I^iPr_2Me_2)_4(\eta^2\text{-}O_2)H]^+$. This outcome is also captured in the computed hydride paramagnetic shielding tensors for $[Ru(IMe_4)_4H]^+$ and $[Ru(IMe_4)_4(\eta^2\text{-}O_2)H]^+$ (see Figure 5). These show a cylindrical tensor for 16e $[Ru(IMe_4)_4H]^+$ which arises from the dominant shielding contributions (in orange) of the two d_π orbitals. In $[Ru(IMe_4)_4(\eta^2\text{-}O_2)H]^+$ the tensor is significantly reduced along one of its principal components and in addition strong deshielding (in blue) is now seen in the parallel direction.

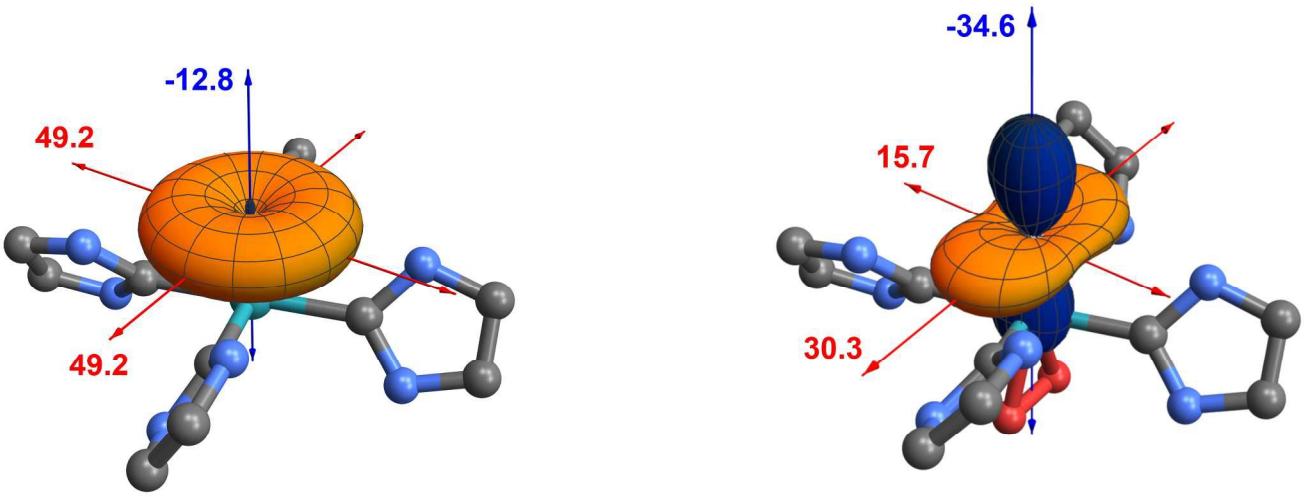

Figure 5. Calculated (ZORA, B1PW91) hydride paramagnetic shielding tensors for $[Ru(IMe_4)_4H]^+$ (left) and $[Ru(IMe_4)_4(\eta^2\text{-}O_2)H]^+$ (right) represented as polar plots[30] of functions $s\sum_{i,j} r_i\sigma_{ij}^p r_j$ where s is a scaling factor (left: s=4, right: s=7) color coded by the sign of σ: orange indicates shielding and blue deshielding. The arrows represent the principal components and the total contributions along each component are indicated. Me groups of the IMe_4 ligands are omitted for clarity.

$[Ru(dippe)_2H]^+$ and $[Ru(dippe)_2(\eta^2\text{-}O_2)H]^+$. Initial calculations were conducted on $[Ru(dmpe)_2H]^+$ and $[Ru(dmpe)_2(\eta^2\text{-}O_2)H]^+$ (where dmpe = $Me_2PCH_2CH_2PMe_2$) and B3PW91 calculations with the

View Article Online
DOI: 10.1039/C7DT00117G

X2C Hamiltonian provided δ_{iso}^{X2C} values of -41.4 ppm and -6.9 ppm respectively. The latter agrees well with experiment for $[Ru(dippe)_2(\eta^2\text{-}O_2)H]^+$ (-6.2 ppm), but for $[Ru(dmpe)_2H]^+$ the calculated hydride chemical shift is 9 ppm more shielded than observed for $[Ru(dippe)_2H]^+$.[7a, 31, 32] One explanation is that some additional interaction is present at the sixth coordination site in $[Ru(dippe)_2H]^+$ that is not captured by the dmpe model. To probe this assertion a $[Ru(dmpe)(dmpe')H]^+$ model was employed (where dmpe' = $Me_2PCH_2CH_2PMeEt$) and a series of constrained geometry optimizations varying the Ru···C^β distance to the Et substituent was performed, and the hydride chemical shift computed for each structure. The results are presented in Figure 6, with the computed values of σ_{iso} and its components (σ_{iso}^d, σ_{iso}^p and σ_{iso}^{so}) provided in Table S3 in the Supporting Information. Figure 6 shows that the initial shortening of the Ru···C^β distance from 4.08 Å (the optimized value in the absence of any constraint) to 3.25 Å only has a minor effect on the hydride chemical shift. However, further shortening reduces the shielding dramatically such that δ_{iso}^{X2C} = -23.0 ppm at Ru···C^β = 2.5 Å. At this geometry the computed Ru···H^β and C^β-H^β distances (1.88 Å and 1.14 Å, respectively) are consistent with a significant Ru···H^β-C^β agostic interaction, the net effect of which on the hydride chemical shift is similar to the Cl ligand in **3**. Moreover, depending on the strength of this agostic interaction, an 18 ppm span in the hydride chemical shift can be accessed. Full optimization of the structure of $[Ru(dippe)_2H]^+$ does indeed show evidence for a weak agostic interaction (Ru···C^β = 2.97 Å, Ru···H^β = 2.19 Å, C^β -H^β = 1.13 Å) and this provides a computed hydride chemical shift of -31.8 ppm, in striking agreement with experiment. Thus the hydride chemical shift in this formally unsaturated species is highly sensitive to the presence of even a weak agostic interaction.

View Article Online
DOI: 10.1039/C7DT00117G

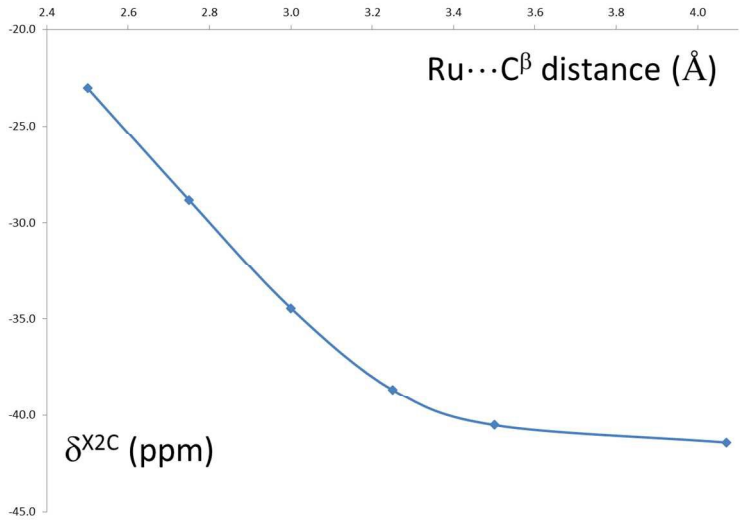

Figure 6. Plot of computed hydride chemical shift (B3PW91, X2C) *vs*. Ru···C$^{\beta}$ distance in the [Ru(dmpe)(dmpe')H]$^{+}$ model system.

The individual components making up σ_{iso} for [Ru(dmpe)$_2$H]$^{+}$, [Ru(dmpe)(dmpe')H]$^{+}$ (Ru···C$^{\beta}$ = 2.5 Å) and [Ru(dippe)$_2$H]$^{+}$ are compared in Figure 7. As seen for the NHC complexes, the major effect upon occupying the 6th coordination site is to reduce the shielding arising from the $\sigma_{\perp}^{p}$ component of the σ_{iso}^{p} term. Thus even the weak coordination of the C$^{\beta}$-H$^{\beta}$ bond destabilizes the $\sigma^{*}_{Ru\text{-}H}$ orbital enough to significantly reduce the contribution of the $\{d_{\pi}|\sigma^{*}_{Ru\text{-}H}\}$ coupling. This is supported by an NCS analysis which shows the average contribution to the $\sigma_{\perp}^{p}$ shielding from the d_{π} orbitals falls from 43.1 ppm in the fully optimised structure to 26.3 ppm when the Ru···C$^{\beta}$ distance is fixed at 2.50 Å (see Table S4, Supporting Information). As before, the contribution from the σ_{iso}^{so} term also drops as the 6th coordination site is occupied.

View Article Online
DOI: 10.1039/C7DT00117G

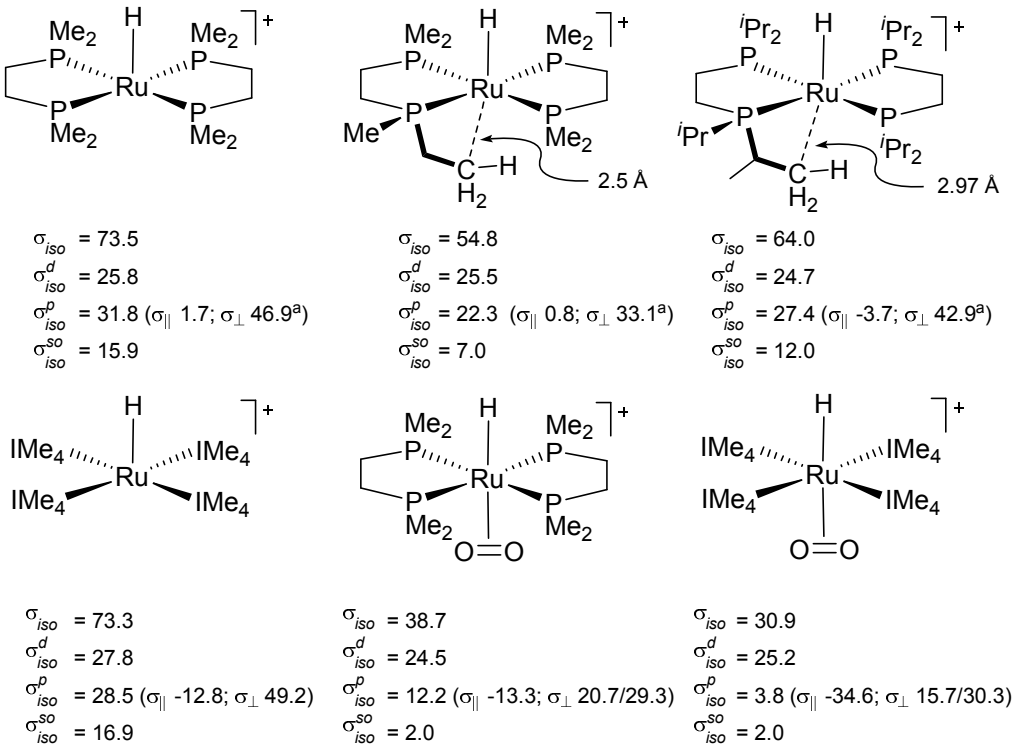

Figure 7. Calculated (B1PW91, ZORA) values for σ_{iso}, σ^{d}_{iso}, σ^{p}_{iso} and σ^{so}_{iso} for selected $[Ru(R_2PCH_2CH_2PR_2)_2(L)H]^+$ species (L = vacant, O_2) along with their $[Ru(IMe_4)_4(L)H]^+$ analogues for comparison. The contributions from $\sigma^{p}_{||}$ and $\sigma^{p}_{\perp}$ are indicated in parenthesis. [a] similar values were obtained for the two components of $\sigma^{p}_{\perp}$ and an average value is indicated.

Comparison of $[Ru(dmpe)_2H]^+$ and $[Ru(IMe_4)_4H]^+$ indicates that the similar values of σ_{iso} actually arise from small variations in its individual components that ultimately cancel each other out. One of the more noticeable differences is in the $\sigma^{p}_{||}$ term which is rather small for $[Ru(dmpe)_2H]^+$ (1.7 ppm) but contributes significant deshielding in $[Ru(IMe_4)_4H]^+$ (-12.8 ppm). The $\sigma^{p}_{||}$ term shows intermediate deshielding in $[Ru(dippe)_2H]^+$ (-3.7 ppm) and so this effect may be associated with variation in the ligand donor strength (dmpe < dippe < NHC). The $\{d_{xy}|d_{x^2-y^2}\}$ coupling will contribute to this deshielding and an NCS analysis indicates that while this component is reduced in

View Article Online
DOI: 10.1039/C7DT00117G

$[Ru(dmpe)_2H]^+$ (-9.8 ppm) it does remain significant; for comparison values of around -15 ppm are computed for $[Ru(dippe)_2H]^+$ and $[Ru(IMe_4)_4H]^+$ (see Table S4, Supporting Information). Other orbital couplings must therefore contribute to diminish the $\sigma^p_{||}$ term in $[Ru(dmpe)_2H]^+$ but the NCS analysis suggests this is an accumulative effect of several contributions rather than any easily identifiable orbital coupling.

A similar effect accounts for the more shielded hydride chemical shift of $[Ru(dmpe)_2(\eta^2\text{-}O_2)H]^+$ compared to $[Ru(IMe_4)_4(\eta^2\text{-}O_2)H]^+$. These species have similar contributions to shielding via the $\sigma^p_{\perp}$ term: for $[Ru(IMe_4)_4(\eta^2\text{-}O_2)H]^+$ this is then effectively cancelled out by $\sigma^p_{||}$ (-34.6 ppm) while for $[Ru(dmpe)_2(\eta^2\text{-}O_2)H]^+$ the $\sigma^p_{||}$ term is only -13.3 ppm and so σ^p_{iso} still contributes to a significant shielding. Closer analysis of these differences proved difficult, however overall it is the contribution of the $\sigma^p_{||}$ term that appears to distinguish the phosphine and NHC complexes studied here and so lies behind the different chemical shifts of the O_2 adducts.

Conclusions

Hydride NMR chemical shifts for a series of $[Ru(IMe_4)_4(L)H]^{0/+}$ species (L = vacant, H_2, N_2, CO, MeCN, O_2, P_4, SO_2, H^-, F^- and Cl^-) have been modelled using relativistic density functional theory. A good correlation between experimental and computed data is obtained with a scalar relativistic correction, however, the inclusion of spin-orbit effects provides much improved quantitative agreement. Analysis of the isotropic shielding indicates that variations in the paramagnetic term, reinforced by changes in the spin-orbit contribution, account for the wide variation in hydride chemical shifts observed in these systems. A natural chemical shift analysis performed for L = vacant, CO, H^-, Cl^- and O_2 identifies the major orbital contributions to the paramagnetic term and links variations in

View Article Online
DOI: 10.1039/C7DT00117G

the shielding of the ^{1}H nucleus to changes in the energies of the occupied Ru d_π orbitals and the unoccupied $\sigma^*_{Ru\text{-}H}$ orbital. In $[Ru(IMe_4)_4(\eta^2\text{-}O_2)H]^+$ the δ-interaction of the O_2 π^*_2 orbital results in one component of the d_π-orbitals (d_{yz}) becoming the relatively low-lying LUMO of the system. This not only precludes any contribution from this orbital to the paramagnetic shielding (as it is no longer occupied), but also switches on additional paramagnetic deshielding via overlap with the occupied d_{xz} orbital under the L_z operator. This combination accounts for the unusually deshielded hydride chemical shift of +4.8 ppm observed for this species.

Calculations also reproduced the change in hydride chemical shift in the related phosphine analogue $[Ru(^iPr_2PCH_2CH_2P^iPr_2)_2(\eta^2\text{-}O_2)H]^+$ (δ = -6.2 ppm). This is linked to changes in the $\sigma_{||}$ contribution to the paramagnetic term, although no simple orbital basis for this could be identified in this case. In contrast, for $[Ru(R_2PCH_2CH_2PR_2)_2H]^+$ species the hydride chemical shift observed experimentally (*ca*. -32 ppm, R = ^{i}Pr, Cy) is clearly dependent on the presence of a weak agostic interaction trans to the hydride ligand and involving one of the phosphine alkyl substituents. In the absence of such an interaction (e.g. R = Me) the calculations predict a similar chemical shift to the $[Ru(IMe_4)_4H]^+$ analogue (ca -41 ppm). Depending on the strength of the agostic interaction a variation of up to 18 ppm in hydride chemical shift is possible. Such weak interactions are therefore significant when it comes to interpreting spectroscopic data and this factor can hopefully aid the interpretation of hydride chemical shift data of nominally unsaturated hydride-containing species.

Experimental Section

All manipulations were carried out using standard Schlenk, high vacuum and glovebox techniques using dry and degassed solvents. Solvents were dried and degassed by standard means, while THF-d_8 was vacuum transferred from potassium. $[Ru(PPh_3)_3(Cl)H]$,[33] $[Ru(IMe_4)_4H]BAr^F_4$ [5] and IMe_4 [34] were

View Article Online
DOI: 10.1039/C7DT00117G

prepared according to the literature. NMR spectra were recorded on a Bruker Avance 500 NMR spectrometer and referenced to δ 3.58 (^{1}H) and 25.4 (^{13}C). Phosphorus NMR spectra for **1** were referenced to H_3PO_4 at δ = 0.0. IR spectra were recorded on a Nicolet Nexus FTIR spectrometer. Elemental analyses were performed by Elemental Microanalysis Ltd, Okehampton, Devon, UK.

[Ru(IMe$_4$)$_4$(P$_4$)H]BAr$_4^F$ (1): [Ru(IMe$_4$)$_4$H]BAr$_4^F$ (69 mg, 0.047 mmol) and P_4 (9 mg, 0.073 mmol) were dissolved in 1.5 mL THF in an ampoule fitted with a J. Young's resealable valve. An immediate colour change from purple to orange was observed. The solution was stirred for 5 min and the volatiles then removed. The residue was washed with hexane (3 x 3 mL) to afford **1** as a pale yellow powder. Yield: 47 mg (63%). X-ray quality crystals were grown from THF/hexane. ^{1}H NMR (500 MHz, THF-d_8, 288 K): δ 7.80 (s, 8H, BAr$_4^F$), 7.59 (s, 4H, BAr$_4^F$), 3.10 (s, 12H, NCH_3), 2.99 (s, 12H, NCH_3), 2.08 (s, 12H, NCCH_3), 2.04 (s, 12H, NCCH_3), -5.09 (dq, $^{2}J_{H\text{-}P}$ = 265.6 Hz, $^{3}J_{H\text{-}P}$ = 11.1 Hz, 1H, Ru-*H*); ^{31}P{^{1}H} (202 MHz, THF-d_8, 258 K): δ -394.6 (q, $^{1}J_{P\text{-}P}$ = 210 Hz), -468.6 (d, $^{1}J_{P\text{-}P}$ = 210 HZ); ^{13}C{^{1}H} NMR (125 MHz, THF-d_8, 258 K): δ 192.6 (d, , $^{2}J_{C\text{-}P}$ = 9 Hz, N*C*N), 163.0 (1:1:1:1 q, $^{1}J_{C\text{-}B}$ = 49 Hz, BAr$_4^F$), 135.7 (s, BAr$_4^F$), 130.2 (q, $J_{C\text{-}F}$ = 32 Hz, BAr$_4^F$), 128.9 (s, N*C*CH$_3$), 125.7 (q, $J_{C\text{-}F}$ = 272 Hz, BAr$_4^F$), 122.4 (s, N*C*CH$_3$), 118.4 (s, BAr$_4^F$), 37.1 (s, N*C*H$_3$), 37.0 (s, NCH_3), 35.7 (s, N*C*H$_3$), 35.6 (s, N*C*H$_3$), 9.8 (s, NC*C*H$_3$), 9.7 (s, NC*C*H$_3$); IR (KBr) ν (cm^{-1}): 1927 cm^{-1} (m, RuH); anal. calcd for $C_{60}H_{61}N_8P_4RuBF_{24}$ (1585.91): C 45.55%, H 3,88%, N 7.07%; found: C 45.94%, H 3.88%, N 7.00%.

[Ru(IMe$_4$)$_4$(SO$_2$)H]BAr$^F_4$ (2). [Ru(IMe$_4$)$_4$H]BAr$_4^F$ (30 mg, 0.021 mmol) was dissolved in 0.5 mL THF-d_8 in a J. Young's resealable NMR tube. After freeze-pump-thaw degassing (3 cycles), SO_2 (1 atm) was added, which generated a pink-red solution in time of mixing. Slow diffusion of hexane into the solution afforded 16 mg (51% yield) of **2** as red crystals. ^{1}H NMR (500 MHz, THF-d_8, 298 K): δ 7.79 (s, 8H, BAr$_4^F$), 7.58 (s, 4H, BAr$_4^F$), 3.22 (s, 12H, NCH_3), 2.97 (s, 12H, NCH_3), 2.12 (s, 12H, NCCH_3), 2.07 (s, 12H, NCCH_3), -4.53 (s, 1H, Ru-*H*); ^{13}C{^{1}H} NMR (125 MHz, THF-d_8, 298 K): δ

View Article Online
DOI: 10.1039/C7DT00117G

185.0 (s, N*C*N), 163.1 (1:1:1:1 q, $^{1}J_{C\text{-}B}$ = 49 Hz, BAr_4^F), 135.8 (s, BAr_4^F), 130.3 (q, $J_{C\text{-}F}$ = 31 Hz, BAr_4^F), 126.6 (s, N*C*CH_3), 126.5 (s, N*C*CH_3), 125.7 (q, $J_{C\text{-}F}$ = 273 Hz, BAr_4^F), 118.4 (s, BAr_4^F), 36.4 (s, N*C*H_3), 35.6 (s, N*C*H_3), 9.8 (s, NC*C*H_3), 9.7 (s, NC*C*H_3); IR (KBr) ν (cm^{-1}): 1919 (m, RuH), 1237 (m, SO_2), 1072 (m, SO_2); anal. calcd for $C_{60}H_{61}N_8RuBF_{24}SO_2$ (1526.34): C 47.22%, H 4.03%, N 7.34%; found: C 47.12%, H 4.24%, N 7.36%.

[Ru(IMe$_4$)$_4$(Cl)H] (3). [Ru(PPh$_3$)$_3$(Cl)H] (200 mg, 0.21 mmol) and IMe$_4$ (118 mg, 0.95 mmol) were suspended in 3 mL THF in an ampoule fitted with a J. Young's resealable tap and the mixture heated at 343 K for 1 h. The yellow suspension was filtered by cannula, the residue washed with Et_2O (2 x 5 mL) and dried *in vacuo* to afford **3** as a yellow solid. Yield: 64 mg (58 %). Single crystals suitable for X-ray diffraction were obtained using an alternative route, whereby a dilute THF (3 mL) solution of [Ru(IMe$_4$)$_4$H$_2$] (20 mg, 0.033 mmol)[25] and $C_6H_5CH_2Cl$ (4 μL, 0.035 mmol) was left to stand for 4 days at room temperature. ^{1}H NMR (500 MHz, THF-d_8, 298 K): δ 3.50 (s, 12H, NCH_3), 3.00 (s, -12H, NCH_3), 2.00 (s, 24H, NCCH_3), -22.62 (s, 1H, Ru*H*); anal. calcd for $C_{28}H_{49}N_8ClRu$ (634.27): C 53.03%, H 7.79%, N 17.66%; found: C 53.07%, H 7.66%, N 17.60%.

Crystallography. Single crystals of compounds **1** and **2** were analysed on a Nonius Kappa CCD diffractometer using Mo(Kα) radiation, while data for **3** were collected using an Agilent SuperNova diffractometer and Cu(Kα) radiation. All analyses were conducted at 150 K. Details of the data collections, solutions and refinements are given in Table S1. The structures were uniformly solved using SHELXS-97[35] and refined using full-matrix least squares in SHELXL-97[36] via the Olex-2 software suite. Refinements were uneventful and only noteworthy details follow. The asymmetric unit in compound **1** was seen to contain one molecule of THF and one molecule of hexane in addition to one molecule of the salt. Of the anion CF_3 groups, fluorine atoms F1-3 and F7-9 were modelled to account for 64:40 and 80:20 disorder, respectively. C-F and F…F distances therein were restrained in the final-least squares cycles and atomic displacement parameter (ADP) restraints were included for

View Article Online
DOI: 10.1039/C7DT00117G

the partial-occupancy atoms F7-9 and F7A-F9A. The hexane ADPs were also refined subject to restraints. Unfortunately, the hydride ligand in the cation could not be reliably located in this structure and, hence, it was omitted from the refinement. In compound **2**, the asymmetric unit was seen to consist of two independent cation halves and two independent anion halves. Ru1, Ru2, B1, B2, H, H1a, S1 and S2 are all coincident with a crystallographic 2-fold rotation axes which serves to generate the remainder of each species present. The refinement of this structure takes account of 90:10 disorder pertaining to Ru1, S1 and O2 with, respectively, Ru1a, S1A and O1A. Ru1 and Ru1a restrained to having similar ADPs in the final least-squares cycles. The hydrides (H1 and H1a) were located and refined at a distance of 1.6 Å from Ru1 and Ru2 respectively. No attempt was made to partition H1a over 2 sites in parallel with the disorder. The asymmetric unit in **3** was seen to comprise one quarter of a molecule, with atoms Ru1, Cl1 and hydride (H1) are located on a crystallographic 4-fold rotation axis. H1 was readily located and refined at a distance of 1.6 Å from the metal Ru1.

Crystallographic data for all compounds have been deposited with the Cambridge Crystallographic Data Centre as supplementary publications CCDC 1462890-2 for **1**, **2** and **3**, respectively. Copies of the data can be obtained free of charge on application to CCDC, 12 Union Road, Cambridge CB2 1EZ, UK [fax(+44) 1223 336033, e-mail: deposit@ccdc.cam.ac.uk.

Computational Details

All geometry optimizations were performed with the Gaussian09 package[37] at the BP86 level.[38] Ru was represented by the relativistic effective core potential (RECP) from the Stuttgart group and the associated basis sets.[39] P and Cl were represented by RECP from the Stuttgart group and the associated basis set,[40] augmented by a d polarization function.[41] The remaining atoms (C, H, N, O, F) were represented by a 6-31G(d,p) basis set.[42] For the NMR calculations, relativistic calculations were carried out with the B3PW91 functional[43] and the 2013 version of the DIRAC

View Article Online
DOI: 10.1039/C7DT00117G

program package,[44] using an exact 2-component Hamiltonian,[45] including spin–orbit coupling, where, in the latter case, two-electron same-spin-orbit corrections were obtained by an atomic mean-field integral (AMFI) approximation.[46] The London orbital formalism (also known as the GIAO framework) has been used for the shielding calculations. The H atoms directly involved in the NMR parameter of interest have been treated with the pcS-2 basis set of Jensen for the chemical shift calculations.[47] The Ru atom was treated with the V2Z basis set of Dyall,[48] whereas the remaining atoms were described with a 6-31G(d,p) basis set. The basis sets for the Dirac calculations were fully decontracted. NMR calculations were also performed within the GIAO framework using ADF 2016[49] with the one-parameter B1PW91 functional[43b, 50] and Slater-type basis sets of triple-ζ (TZP) quality. Relativistic effects were treated by the 2-component zeroth-order regular approximation (ZORA),[51] and the response of the first-order exchange-correlation potential was included for the calculated NMR shielding tensors.[52] Analysis of scalar-relativistic natural localized molecular orbitals were done with the NBO 6.0 program.[53] NMR shielding tensors calculated with ADF were analysed using these scalar-relativistic NLMO.

Acknowledgements

Financial support was provided by the EPSRC (LJLH, EP/F029039/1) and through a DTA studentship (MKC), the Spanish Ministerio de Ciencia e Innovación (EMM), the University of Bristol (RAS) and the Royal Society for an International Exchange Award (SAM, CR). We thank Johnson Matthey plc for the loan of some of the hydrated ruthenium trichloride. This computational work was performed using HPC resources of CINES and IDRIS under the allocation 2016-087529 made by GENCI. Prof. Odile Eisenstein is acknowledged for many fruitful discussions.

Supporting Information

View Article Online
DOI: 10.1039/C7DT00117G

NMR spectra and X-ray details for compounds **1**, **2** and **3**; computed ^{1}H chemical shifts for $[Ru(IMe_4)_4(L)H]^{0/+}$ and $[Ru(R_2PCH_2CH_2PR_2)_2(L)H]^{+}$ species; NCS Analysis for $[Ru(R_2PCH_2CH_2PR_2)_2(L)H]^{+}$ species; optimised structures and energies of all species.

References

1. (a) J. Choi, A. H. R. MacArthur, M. Brookhart and A. S. Goldman, *Chem. Rev.*, 2011, 111, 1761-1779; (b) S. E. Clapham, A. Hadzovic and R. H. Morris, *Coord. Chem. Rev.*, 2004, 248, 2201-2237; (c) H. D. Kaesz and R. B. Saillant, *Chem. Rev.*, 1972, 72, 231-281; (d) F. Kakiuchi and S. Murai, *Acc. Chem. Res.*, 2002, 35, 826-834; (e) G. J. Kubas, *Catal. Lett.*, 2005, 104, 79-101; (f) R. N. Perutz and S. Sabo-Etienne, *Angew. Chem. Int. Ed.*, 2007, 46, 2578-2592; (g) J. S. M. Samec, J.-E. Bäckvall, P. G. Andersson and P. Brandt, *Chem. Soc. Rev.*, 2006, 35, 237-248; (h) A. E. Shilov and G. B. Shul'pin, *Chem. Rev.*, 1997, 97, 2879-2932.
2. (a) R. H. Morris, *Coord. Chem. Rev.*, 2008, 252, 2381-2394; (b) P. S. Pregosin, *NMR in Organometallic Chemistry*, Wiley-VCH, Weinheim, 2012.
3. NHC abbreviations: $I^{i}Pr_2Me_2$ = 1,3-diisopropyl-4,5-dimethylimidazol-2-ylidene, IEt_2Me_2 = 1,3-diethyl-4,5-dimethylimidazol-2-ylidene, IMe_4 = 1,3,4,5-tetramethylimidazol-2-ylidene.
4. L. J. L. Häller, E. Mas-Marzá, A. Moreno, J. P. Lowe, S. A. Macgregor, M. F. Mahon, P. S. Pregosin and M. K. Whittlesey, *J. Am. Chem. Soc.*, 2009, 131, 9618-9619.
5. S. Burling, L. J. L. Häller, E. Mas-Marza, A. Moreno, S. A. Macgregor, M. F. Mahon, P. S. Pregosin and M. K. Whittlesey, *Chem.-Eur. J.*, 2009, 15, 10912-10923.
6. (a) P. Hrobárik, V. Hrobáriková, F. Meier, M. Repiský, S. Komorovský and M. Kaupp, *J. Phys. Chem. A*, 2011, 115, 5654-5659; (b) M. Kaupp and O. L. Malkina, *J. Chem. Phys.*, 1998, 108, 3648-3659.
7. (a) M. Jiménez-Tenorio, M. C. Puerta and P. Valerga, *J. Am. Chem. Soc.*, 1993, 115, 9794-9795; (b) M. Jiménez-Tenorio, M. C. Puerta and P. Valerga, *Inorg. Chem.*, 1994, 33, 3515-3520.
8. M. Kaupp, M. Buehl and V. G. Malkin, *NMR and EPR Parameters: Theory and Applications;* , Wiley-VCH, Weinheim, 2006.
9. Y. Ruiz-Morales, G. Schreckenbach and T. Ziegler, *Organometallics*, 1996, 15, 3920-3923.
10. (a) A. D. Buckingham and P. J. Stephens, *J. Chem. Soc.*, 1964, 2747-2759; (b) A. D. Buckingham and P. J. Stephens, *J. Chem. Soc.*, 1964, 4583-4587.
11. (a) A. Bhattacharjee, M. Chavarot-Kerlidou, E. S. Andreiadis, M. Fontecave, M. J. Field and V. Artero, *Inorg. Chem.*, 2012, 51, 7087-7093; (b) I. del Rosal, L. Maron, R. Poteau and F. Jolibois, *Dalton Trans.*, 2008, 3959-3970; (c) R. Gobetto, C. Nervi, B. Romanin, L. Salassa, M. Milanesio and G. Croce, *Organometallics*, 2003, 22, 4012-4019.
12. (a) M. A. M. Al-Ibadi, S. B. Duckett and J. E. McGrady, *Dalton Trans.*, 2012, 41, 4618-4625; (b) I. del Rosal, F. Jolibois, L. Maron, K. Philippot, B. Chaudret and R. Poteau, *Dalton Trans.*, 2009, 2142-2156; (c) A. S. Estrada-Montano, M. A. Leyva, R. Grande-Aztatzi, A. Vela and M. J. Rosales-Hoz, *J. Organomet. Chem.*, 2014, 751, 420-429; (d) For calculations of $^{1}J_{H\text{-}D}$ coupling constants in a range of transition metal η^2-HD and (H)(D) complexes see: (e) B. Le Guennic, S. Patchkovskii and J. Autschbach, *J. Comput. Theor. Chem.*, 2005, 1, 601-611.

View Article Online
DOI: 10.1039/C7DT00117G

13. (a) J. Autschbach, *J. Chem. Phys.*, 2012, 136; (b) T. Helgaker, M. Jaszuński and K. Ruud, *Chem. Rev.*, 1999, 99, 293-352; (c) P. Pyykkö, *Ann. Rev. Phys. Chem.*, 2012, 63, 45-64.
14. (a) A. Bagno and G. Saielli, *Phys. Chem. Chem. Phys.*, 2011, 13, 4285-4291; (b) P. Garbacz, V. V. Terskikh, M. J. Ferguson, G. M. Bernard, M. Kędziorek and R. E. Wasylishen, *J. Phys. Chem. A*, 2014, 118, 1203-1212.
15. S. Halbert, C. Copéret, C. Raynaud and O. Eisenstein, *J. Am. Chem. Soc.*, 2016, 138, 2261-2272.
16. (a) V. Mirabello, M. Caporali, V. Gallo, L. Gonsalvi, D. Gudat, W. Frey, A. Ienco, M. Latronico, P. Mastrorilli and M. Peruzzini, *Chem.-Eur. J.*, 2012, 18, 11238-11250; (b) V. Mirabello, M. Caporali, V. Gallo, L. Gonsalvi, A. Ienco, M. Latronico, P. Mastrorilli and M. Peruzzini, *Dalton Trans.*, 2011, 40, 9668-9671.
17. O. Kühl, *Phosphorus-31 NMR Spectroscopy - A Concise Introduction for the Synthetic Organic and Organometallic Chemist*, Springer, Heidelberg, 2008.
18. (a) For other examples of fluxional processes involving P_4 ligands see Ref 16(a) and (b) L. C. Forfar, D. Zeng, M. Green, J. E. McGrady and C. A. Russell, *Chem.-Eur. J.*, 2016, 22, 5397-5403.
19. G. J. Kubas, *Inorg. Chem.*, 1979, 18, 182-188.
20. (a) R. R. Ryan and G. J. Kubas, *Inorg. Chem.*, 1978, 17, 637-641; (b) S. Tampier, R. Müller, A. Thorn, E. Hübner and N. Burzlaff, *Inorg. Chem.*, 2008, 47, 9624-9641.
21. Acetonitrile displaced the chloride ligand to form the known $[Ru(IMe_4)_4(MeCN)H]^+$, while dissolution in dichloromethane gave the dichloride $[Ru(IMe_4)_4Cl_2]$.
22. (a) R. G. Ball, B. R. James, J. Trotter, D. K. W. Wang and K. R. Dixon, *J. Chem. Soc., Chem. Comm.*, 1979, 460-461; (b) G. R. Clark, A. Falshaw, G. J. Gainsford, C. Lensink, A. T. Slade and L. J. Wright, *J. Coord. Chem.*, 2010, 63, 373-393; (c) B. Delavaux, B. Chaudret, J. Devillers, F. Dahan, G. Commenges and R. Poilblanc, *J. Am. Chem. Soc.*, 1986, 108, 3703-3711; (d) J. Figueira, M. G. Jardim, J. Rodrigues, A. Valkonen and K. Rissanen, *Inorg. Chem. Commun.*, 2013, 29, 123-127; (e) J. Shen, E. D. Stevens and S. P. Nolan, *Organometallics*, 1998, 17, 3875-3882.
23. R. Wolf, M. Plois and A. Hepp, *Eur. J. Inorg. Chem.*, 2010, 918-925.
24. E. R. Johnson, S. Keinan, P. Mori-Sánchez, J. Contreras-García, A. J. Cohen and W. Yang, *J. Am. Chem. Soc.*, 2010, 132, 6498-6506.
25. M. K. Cybulski, D. McKay, S. A. Macgregor, M. F. Mahon and M. K. Whittlesey, *Angew. Chem. Int. Ed.*, 2017, 56, 1515-1519.
26. Wolf and coworkers have previously computed a similar geometry for trans-$[Ru(IMe_4)_4H_2]$ using a BP86-D protocol. See Ref 23.
27. (a) J. Autschbach and S. Zheng, *Magn. Reson. Chem.*, 2008, 46, S45-S55; (b) C. D. Cornwell, *J. Chem. Phys.*, 1966, 44, 874-880; (c) C. J. Jameson and H. S. Gutowsky, *J. Chem. Phys.*, 1964, 40, 1714-1724.
28. (a) J. A. Bohmann, F. Weinhold and T. C. Farrar, *J. Chem. Phys.*, 1997, 107, 1173-1184; (b) J. Autschbach, *J. Chem. Phys.*, 2008, 128, 164112; (c) F. Aquino, B. Pritchard and J. Autschbach, *J. Comput. Theor. Chem.*, 2012, 8, 598-609; (d) For convenience, we refer to this NLMO analysis of shielding as the Natural Chemical Shift (NCS) analysis using the terminology proposed in the original work by Weinhold[28a] and subsequently elaborated by Autschbach.[28b,c].
29. M. Kaupp, O. L. Malkina, V. G. Malkin and P. Pyykkö, *Chem.-Eur. J.*, 1998, 4, 118-126.
30. (a) J. Autschbach, S. Zheng and R. W. Schurko, *Concepts in Magnetic Resonance Part A*, 2010, 36A, 84-126; (b) E. Zurek, C. J. Pickard and J. Autschbach, *J. Phys. Chem. C*, 2008, 112, 11744-11750.

View Article Online
DOI: 10.1039/C7DT00117G

31. The formation of $[Ru(dmpe)_2H]^+$ has been postulated upon treatment of cis-$[Ru(dmpe)_2(H)_2]$ in methanol.[32] However the large discrepancy between the reported ^1H chemical shift of -25.9 ppm and the computed value of -41 ppm suggests an alternative formulation, possibly a MeOH adduct $[Ru(dmpe)_2(MeOH)H]^+$.
32. L. D. Field, T. W. Hambley and B. C. K. Yau, *Inorg. Chem.*, 1994, 33, 2009-2017.
33. R. A. Schunn, E. R. Wonchoba and W. G, *Inorg. Synth.*, 1971, 13, 131-134.
34. N. Kühn and T. Kratz, *Synthesis*, 1993, 561-563.
35. G. M. Sheldrick, *SHELXL-97, a Computer Program for Crystal Structure Refinement*, University of Göttingen, 1997.
36. G. M. Sheldrick, *Acta Crystallographica* 1990, A46, 467-473.
37. M. J. Frisch, G. W. Trucks, H. B. Schlegel, G. E. Scuseria, M. A. Robb, J. R. Cheeseman, J. J. A. Montgomery, T. Vreven, K. N. Kudin, J. C. Burant, J. M. Millam and J. T. S. S. Iyengar, V. Barone, B. Mennucci, M. Cossi, G. Scalmani, N. Rega, G. A. Petersson, H. Nakatsuji, M. Hada, M. Ehara, K. Toyota, R. Fukuda, J. Hasegawa, M. Ishida, T. Nakajima, Y. Honda, O. Kitao, H. Nakai, M. Klene, X. Li, J. E. Knox, H. P. Hratchian, J. B. Cross, V. Bakken, C. Adamo, J. Jaramillo, R. Gomperts, R. E. Stratmann, O. Yazyev, A. J. Austin, R. Cammi, C. Pomelli, J. W. Ochterski, P. Y. Ayala, K. Morokuma, G. A. Voth, P. Salvador, J. J. Dannenberg, V. G. Zakrzewski, S. Dapprich, A. D. Daniels, M. C. Strain, O. Farkas, D. K. Malick, A. D. Rabuck, K. Raghavachari, J. B. Foresman, J. V. Ortiz, Q. Cui, A. G. Baboul, S. Clifford, J. Cioslowski, B. B. Stefanov, G. Liu, A. Liashenko, P. Piskorz, I. Komaromi, R. L. Martin, D. J. Fox, T. Keith, M. A. Al-Laham, C. Y. Peng, A. Nanayakkara, M. Challacombe, P. M. W. Gill, B. Johnson, W. Chen, M. W. Wong, C. Gonzalez, and J. A. Pople, Gaussian, Inc., Wallingford CT, 2013.
38. (a) A. D. Becke, *Phys. Rev. A*, 1988, 38, 3098-3100; (b) J. P. Perdew, *Phys. Rev. B*, 1986, 33, 8822-8824.
39. D. Andrae, U. Häussermann, M. Dolg, H. Stoll and H. Preuss, *Theor. Chim. Acta*, 1990, 77, 123-141.
40. A. Bergner, M. Dolg, W. Küchle, H. Stoll and H. Preuss, *Mol. Phys.*, 1993, 80, 1431-1441.
41. A. Höllwarth, M. Böhme, S. Dapprich, A. W. Ehlers, A. Gobbi, V. Jonas, K. F. Köhler, R. Stegmann, A. Veldkamp and G. Frenking, *Chem. Phys. Lett.*, 1993, 208, 237-240.
42. (a) P. C. Hariharan and J. A. Pople, *Theor. Chim. Acta*, 1973, 28, 213-222; (b) W. J. Hehre, R. Ditchfield and J. A. Pople, *J. Chem. Phys.*, 1972, 56, 2257-2261.
43. (a) A. D. Becke, *J. Chem. Phys.*, 1993, 98, 5648-5652; (b) J. P. Perdew and Y. Wang, *Phys. Rev. B*, 1992, 45, 13244-13249.
44. DIRAC, a relativistic ab initio electronic structure program, Release DIRAC13 (2013), written by L. Visscher, H. J. Aa. Jensen, R. Bast, and T. Saue, with contributions from V. Bakken, K. G. Dyall, S. Dubillard, U. Ekström, E. Eliav, T. Enevoldsen, E. Faßhauer, T. Fleig, O. Fossgaard, A. S. P. Gomes, T. Helgaker, J. K. Lærdahl, Y. S. Lee, J. Henriksson, M. Iliaš, Ch. R. Jacob, S. Knecht, S. Komorovský, O. Kullie, C. V. Larsen, H. S. Nataraj, P. Norman, G. Olejniczak, J. Olsen, Y. C. Park, J. K. Pedersen, M. Pernpointner, K. Ruud, P. Sałek, B. Schimmelpfennig, J. Sikkema, A. J. Thorvaldsen, J. Thyssen, J. van Stralen, S. Villaume, O. Visser, T. Winther, and S. Yamamoto (see http://www.diracprogram.org).
45. M. Iliaš and T. Saue, *J. Chem. Phys.*, 2007, 126, 064102.
46. (a) B. Schimmelpfennig, *AMFI: An Atomic Mean Field Code, Stockholm, Sweden, 1996*; (b) B. A. Hess, C. M. Marian, U. Wahlgren and O. Gropen, *Chem. Phys. Lett.*, 1996, 251, 365-371.
47. F. Jensen, *J. Comput. Theor. Chem.*, 2008, 4, 719-727.
48. K. G. Dyall, *Theor. Chem. Acc.*, 2007, 117, 483-489.

View Article Online
DOI: 10.1039/C7DT00117G

49. (a) ADF2016, SCM, Theoretical Chemistry, Vrije Universiteit, Amsterdam, The Netherlands, http://www.scm.com; (b) G. t. Velde, F. M. Bickelhaupt, E. J. Baerends, C. F. Guerra, S. J. A. v. Gisbergen, J. G. Snijders and T. Ziegler, *J. Comput. Chem.*, 2001, 22, 931-967; (c) C. F. Guerra, J. G. Snijders, G. te Velde and E. J. Baerends, *Theor. Chem. Acc.*, 1998, 99, 391-403.
50. A. D. Becke, *J. Chem. Phys.*, 1996, 104, 1040-1046.
51. (a) G. Schreckenbach and T. Ziegler, *J. Phys. Chem.*, 1995, 99, 606-611; (b) M. Krykunov, T. Ziegler and E. v. Lenthe, *Int. J. Quant. Chem.*, 2009, 109, 1676-1683.
52. J. Autschbach, *Mol. Phys.*, 2013, 111, 2544-2554.
53. NBO 6.0. E. D. Glendening, J. K. Badenhoop, A. E. Reed, J. E. Carpenter, J. A. Bohmann, C. M. Morales, C. R. Landis, and F. Weinhold (Theoretical Chemistry Institute, University of Wisconsin, Madison, WI, 2013); http://nbo6.chem.wisc.edu/.

View Article Online
DOI: 10.1039/C7DT00117G

Table of Contents Graphic

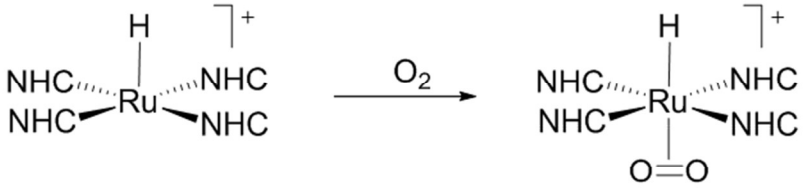

Experiment: $^1H\ \delta = -41$ ppm $^1H\ \delta = +4.8$ ppm

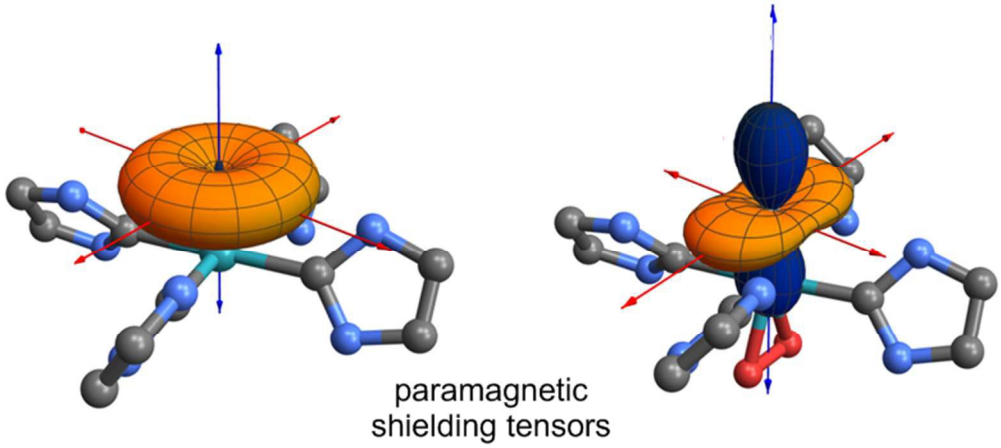

Computation: $\sigma^p_{iso} = +28.5$ ppm $\sigma^p_{iso} = +3.8$ ppm